Precipitation response to land subsurface hydrologic processes in atmospheric general circulation model simulations

Min-Hui Lo[1,2] and James S. Famiglietti[1,2]

Received 30 September 2010; revised 22 December 2010; accepted 30 December 2010; published 5 March 2011.

[1] Several studies have established that soil moisture increases after adding a groundwater component in land surface models, owing to the additional supply of subsurface water. However, the impact of groundwater on the spatial-temporal variability of precipitation has received little attention. This study explores how a groundwater representation in land surface models alters precipitation distributions through coupled groundwater-land-atmosphere simulations. Results indicate that the addition of groundwater yields a global increase in soil water content and evapotranspiration, a decrease in surface air temperature, and an increase in cloud cover fraction. These result in globally inhomogeneous changes in precipitation. In the boreal summer, tropical land regions show a positive anomaly in the Northern Hemisphere and a negative anomaly in the Southern Hemisphere. As a result, an asymmetric dipole is found over tropical land regions along the equator. Furthermore, in the transition climatic zone where the land and atmosphere are strongly coupled, precipitation also increases. Two main mechanisms are suggested for the two different regions with increased precipitation. The "rich-get-richer" mechanism is responsible for the positive precipitation anomalies over the tropical land regions, while a positive feedback of land-atmosphere interaction is the major contributor to increased precipitation over central North America. This study highlights the importance of land subsurface hydrologic processes in the climate system and has further implications for global water cycle dynamics.

Citation: Lo, M.-H., and J. S. Famiglietti (2011), Precipitation response to land subsurface hydrologic processes in atmospheric general circulation model simulations, *J. Geophys. Res.*, *116*, D05107, doi:10.1029/2010JD015134.

1. Introduction and Background

[2] Unlike the ocean, which has an infinite water supply, the supply of moisture on land is limited and highly variable. Hence land hydrology becomes critical in determining moisture supply to the atmosphere through the process of evapotranspiration. *Manabe* [1969] used an interactive bucket model to provide a lower boundary condition for climate model simulations, pioneering the idea of adding a parameterization of the land surface in general circulation models (GCMs). Since then, significant improvements in land surface models (LSMs) have been made. For example, *Dickinson et al.* [1986] and *Sellers et al.* [1986] developed Soil-Vegetation-Atmosphere Transfer (SVAT) schemes to describe fluxes of energy, water, and momentum between the atmosphere and land surface. Others [e.g., *Entekhabi and Eagleson*, 1989; *Famiglietti and Wood*, 1991, 1994] have used a statistical-dynamical framework to account for subgrid heterogeneity within a model grid.

[3] These and other models have shown that variations of surface air temperature over land are larger in experiments with interactive soil moisture than those using prescribed soil moisture [*Delworth and Manabe*, 1993]. Positive soil moisture–rainfall feedbacks have been observed in Illinois [*Findell and Eltahir*, 1997; *D'Odorico and Porporato*, 2004], in Kansas [*Eltahir*, 1998], and across the U.S. [*Koster et al.*, 2003]. *Koster et al.* [2000] have suggested that during summer in midlatitude continental areas, soil moisture becomes more important than sea surface temperature in affecting atmospheric processes. In addition, several studies have pointed to the importance of soil moisture to the atmosphere, and showed that the initialization of soil moisture in a seasonal-to-interannual forecasting system can improve model predictions [e.g., *Koster et al.*, 2000, 2004; *Dirmeyer*, 2001; *Koster and Suarez*, 2001, 2003; *Seneviratne et al.*, 2006; *Teuling et al.*, 2006; *Zhang et al.*, 2008].

[4] Although previous studies have emphasized the importance of soil moisture, the effect of groundwater on land hydrologic processes is not well understood [*Wu and Dickinson*, 2004; *Amenu et al.*, 2005]. Deeper soil moisture and groundwater can play more important roles in hydrologic processes owing to their longer time scales of persistence. Several studies have shown that subsurface

[1]Department of Earth System Science, University of California, Irvine, California, USA.
[2]UC Center for Hydrologic Modeling, University of California, Irvine, California, USA.

0148-0227/11/2010JD015134

hydrologic processes can modulate atmospheric dynamics and processes. For example, *Quinn et al.* [1995] indicated that spatial groundwater variations could make substantial changes in atmospheric boundary layer development. A recent study by *van den Hurk et al.* [2005], who analyzed seven regional climate models, indicated that responses of the hydrologic cycle are usually too fast in models owing to insufficient soil water storage. *Güntner et al.* [2007] indicated that groundwater tends to have a larger contribution to the interannual mode of total water storage variations than to seasonal variations. Moreover, *Koutsoyiannis et al.* [2007] found that GCM simulated runoff usually has high values of the Hurst coefficient compared to that of historical data. One possible reason is that after adding groundwater processes in runoff generation, simulated runoff could have greater memory.

[5] Recently, the representation of groundwater dynamics in LSMs has begun to receive considerable attention [e.g., *Famiglietti and Wood*, 1991, 1994; *Liang et al.*, 2003; *Maxwell and Miller*, 2005; *Yeh and Eltahir*, 2005a, 2005b; *Fan et al.*, 2007; *Maxwell et al.*, 2007; *Miguez-Macho et al.*, 2007, 2008; *Niu et al.*, 2007; *Lo et al.*, 2008]. These studies have shown the importance of representing shallow groundwater and its interaction with soil moisture in land hydrologic simulations. Groundwater affects the atmosphere by influencing the soil moisture profile and the evapotranspiration rate [e.g., *Gutowski et al.*, 2002; *York et al.*, 2002; *Liang et al.*, 2003; *Chen and Hu*, 2004]. For example, *Gutowski et al.* [2002] developed a Coupled Land-Atmosphere Simulation Program (CLASP) to simulate coupled hydrologic processes, including groundwater flow in a phreatic aquifer. CLASP has the ability to simulate the response of the groundwater table to the recharge flux. They reported that over 30% of monthly evapotranspiration is from groundwater within a simulation domain of 80 km by 80 km near the central U.S., indicating the importance of aquifer-atmosphere interaction.

[6] *Elmore et al.* [2008] showed that groundwater fluctuations could affect dust mobilization by altering land surface properties. Further, analyses of in situ data sets in Illinois have shown that groundwater can have significant impacts on the rate of evapotranspiration during dry seasons [*Yeh and Famiglietti*, 2009]. *Lo and Famiglietti* [2010] found that feedbacks of groundwater on land surface hydrologic memory can be positive, negative, or neutral depending on water table depth. However, the contributions of groundwater to the spatial-temporal variability of precipitation have received little attention; for example, where does precipitation increase when a groundwater representation is included in LSMs and what mechanisms are responsible for these changes? Only a few studies [e.g., *Anyah et al.*, 2008] have reported that the impacts of groundwater on precipitation are highly spatially variable.

[7] Recent work [e.g., *Anyah et al.*, 2008; *Yuan et al.*, 2008; *Jiang et al.*, 2009] has shown that groundwater aquifers can alter simulated land-atmosphere feedbacks in a regional atmospheric model. Still, the precipitation-recycling ratio, which describes the fraction of local precipitation derived from local evapotranspiration, may affect the strength and phase of the influence of groundwater on the atmosphere. Given the one-way nature of the interactions imposed by lateral boundary conditions in regional models, as well as the uncertainty in the boundary forcing, fully coupled land-atmosphere GCMs will be an important step forward in understanding the full role of groundwater in climate system feedbacks.

[8] This study will focus on spatial variations of atmospheric precipitation responses to groundwater and will explore the mechanisms responsible for precipitation changes across regions. A fully coupled model, the NCAR Community Atmosphere Model + Community Land Model + groundwater aquifer, with prescribed sea surface temperature and sea ice concentration, is utilized in this study.

2. Model and Experiment Setup

[9] The coupled model used for this study is the NCAR Community Atmosphere Model, version 3.5 (CAM3.5). Significant modifications and improvements to CAM3.0 are apparent in CAM3.5. For details of the changes, the reader is referred to the work of *Gent et al.* [2009, and references therein]. CAM3.5 includes CLM3.5 [*Oleson et al.*, 2008] with an unconfined groundwater aquifer model [*Niu et al.*, 2007] and the SIMTOP (simple TOPMODEL-based) runoff scheme developed by *Niu et al.* [2005]. For detailed descriptions of the physics in the CLM3.5, the reader is referred to the work of *Oleson et al.* [2008] and *Niu et al.* [2005, 2007]. In this paper, only the groundwater recharge flux is briefly described for the purpose of the model experiment. The groundwater recharge flux in CLM3.5 is described by Darcy's law:

$$q = -k\frac{\partial\left(\psi = \psi_m + \psi_g\right)}{\partial z}$$
$$q_g = -k\frac{\partial\psi_g}{\partial z} = -k\frac{\partial(-z)}{\partial z} = k, \tag{1}$$
$$q_m = -k\frac{\partial\psi_m}{\partial z}$$

where q (mm/s) is the soil water flux (negative upward), k (mm/s) is the hydraulic conductivity, ψ (mm) is the hydraulic potential, and z (mm) is the depth between the water table and the soil layer. The hydraulic potential can be separated into soil water potential (ψ_m) and gravitational potential (ψ_g). The reference level is at the soil surface so ψ_g is equal to the depth ($-z$). The water table is interactively linked to the soil moisture model through the exchange of groundwater recharge (i.e., the sum of the soil drainage flux (q_g) and capillary rise (q_m)) at the bottom of the soil column. The water table depth is computed at each time step using

$$S_y\frac{dH}{dt} = I_{gw} - Q_{gw}, \tag{2}$$

where S_y [ ] is the specific yield of the unconfined aquifer, H [L] is the groundwater level above a datum, I_{gw} [L/T] is groundwater recharge, which is the flux at the interface between the unsaturated and saturated zone, that is, the water table, and Q_{gw} [L/T] is groundwater discharge to streams (i.e., groundwater runoff).

[10] Simulations are performed at the standard T42 resolution (spectral truncation at wave number 42, approximately 2.8° × 2.8°) with 26 vertical hybrid coordinate levels. The simulations are forced by prescribed sea surface temperatures

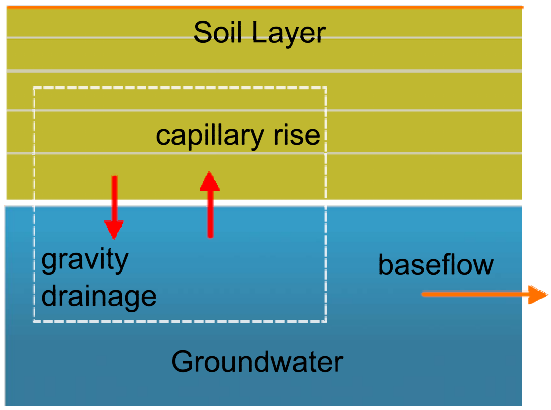

Figure 1. Schematic representation of the interactive linkage between soil moisture and groundwater model through the exchange of the soil drainage flux and capillary rise at the bottom of the soil column.

and sea ice concentrations [*Hurrell et al.*, 2008]. Initial conditions of the water table depth and soil moisture profile are estimated by the fitting approach described by *Lo and Famiglietti* [2010]. In the fitting approach, exponential decay functions are used to fit the time series of the first 100 years of water table depths at each model grid. An equilibrium water table depth is defined as the asymptote of the exponential decay function. After the equilibrium water table depth is found by the fitting approach, vertical soil moisture profiles can be determined from the soil moisture characteristic relationships by *Brooks and Corey* [1964]:

$$\theta(\psi) = \theta_r + (\theta_s - \theta_r)\left(\frac{\psi_{cf}}{\psi}\right)^{1/B}, \quad \psi > \psi_{cf}, \tag{3}$$

where θ ( ) is the soil moisture content, θ_r ( ) is the residual moisture content, θ_s ( ) is the soil moisture content at saturation (i.e., porosity), ψ_{cf} (mm) is the depth of the capillary fringe, and B ( ) is the pore size distribution index.

[11] Two online experiments conducted with CAM3.5 are presented here: a no groundwater run (NO-GW) and a groundwater run (GW). In the NO-GW run, the capillary flux (q_m) from the aquifer to the soil model is inactive. For the GW run, the water table is interactively linked to soil moisture model through the exchange of the soil drainage flux and capillary rise at the bottom of the soil column as shown in Figure 1. As a result, the impacts of groundwater on precipitation can be identified via the differences (anomalies) between the two experiments. The simulation produces 129 years of global monthly output from 1871 to 1999. In order to remove the effects of uncertain initial and boundary conditions, the 1870–1899 period is treated as spin-up, and 100 year (1900–1999) simulations are used in the analysis.

3. Results

3.1. Spatial Variations of Precipitation Responses to Groundwater

[12] Figure 2a shows global (−180° to 180°, 60°S to 60°N) land average precipitation for the GW and NO-GW runs in JJA (June, July, and August) from 1900 to 1999. After adding a groundwater component in the model (the GW run), the model produces more precipitation over land owing to an increase in lower tropospheric (surface to 850 mbar) integrated water vapor (Figure 2d) from an overall increase in top soil water (Figure 2c) and evapotranspiration (Figure 2b). Figure 2e also indicates that near surface air temperature decreases because of less sensible heat release. Besides higher evapotranspiration, a higher cloud cover fraction in the GW run increases the albedo, causing less shortwave radiation to reach the land surface (not shown here). Taken together, the GW run has lower land surface temperature resulting in lower sensible heat release.

[13] The major reason for this increase of precipitation (Figure 2a) is that more water vapor in the lower troposphere increases moist static energy [*Eltahir*, 1998] that further reduces moist static stability [*Chou and Neelin*, 2004], thereby enhancing convection. However, this increase in precipitation is not globally homogeneous as shown in Figure 3a, which shows the spatial pattern of the 100 year average JJA precipitation for the difference between the two runs. Figure 3a clearly portrays asymmetric responses of precipitation anomalies in central Africa and northern South America. A positive anomaly is found in central North America and eastern Europe. Figure 3b shows the 100 year time series of averaged precipitation for the two black outlined boxes in Figure 3a (Zone A and Zone B). A 15 year running mean has been applied to the time series. Zone A and Zone B display opposite evolutionary responses in the precipitation anomalies. This asymmetry feature is more apparent in the difference between the time series (Zone A minus Zone B) in Figure 3c. Below, we discuss the mechanisms responsible for such precipitation changes.

3.2. Decompositions of Precipitation Anomalies

[14] The vertically integrated moisture budget equation is utilized to explore precipitation anomalies induced by groundwater in Figure 3a:

$$\left\langle \frac{\partial q}{\partial t} \right\rangle = ET - P - \langle \nabla \cdot (\mathbf{v}q) \rangle, \tag{4}$$

where q is water vapor, ET is evapotranspiration, P is precipitation, $\mathbf{v}$ is horizontal velocity, and $\langle\ \rangle$ denotes a mass integration throughout the troposphere (i.e., $\frac{1}{g}\int_{p_s}^{p_t}(\ )dp$, where g is gravity, p_t is the pressure at the top of troposphere, and p_s is surface pressure). Since vertical velocity is relatively small at the surface and the top of troposphere [*Tan et al.*, 2008], the divergence of moisture flux can be estimated as follows:

$$\langle \nabla \cdot (\mathbf{v}q) \rangle \approx \langle \mathbf{v} \cdot \nabla q \rangle + \left\langle w \frac{\partial q}{\partial p} \right\rangle, \tag{5}$$

where w is pressure velocity, $\mathbf{v} \cdot \nabla q$ is the horizontal moisture advection, and $w\frac{\partial q}{\partial p}$ is the vertical moisture advection. All the terms are in energy units $\left(\frac{W}{m^2}\right)$. For long-term averages, the time derivative term can be ignored. Precipitation anomalies caused by groundwater can therefore be written as [*Chou and Neelin*, 2004; *Chou et al.*, 2006]

$$P' \approx ET' - \langle \mathbf{v} \cdot \nabla q \rangle' - \left\langle w \frac{\partial q}{\partial p} \right\rangle', \tag{6}$$

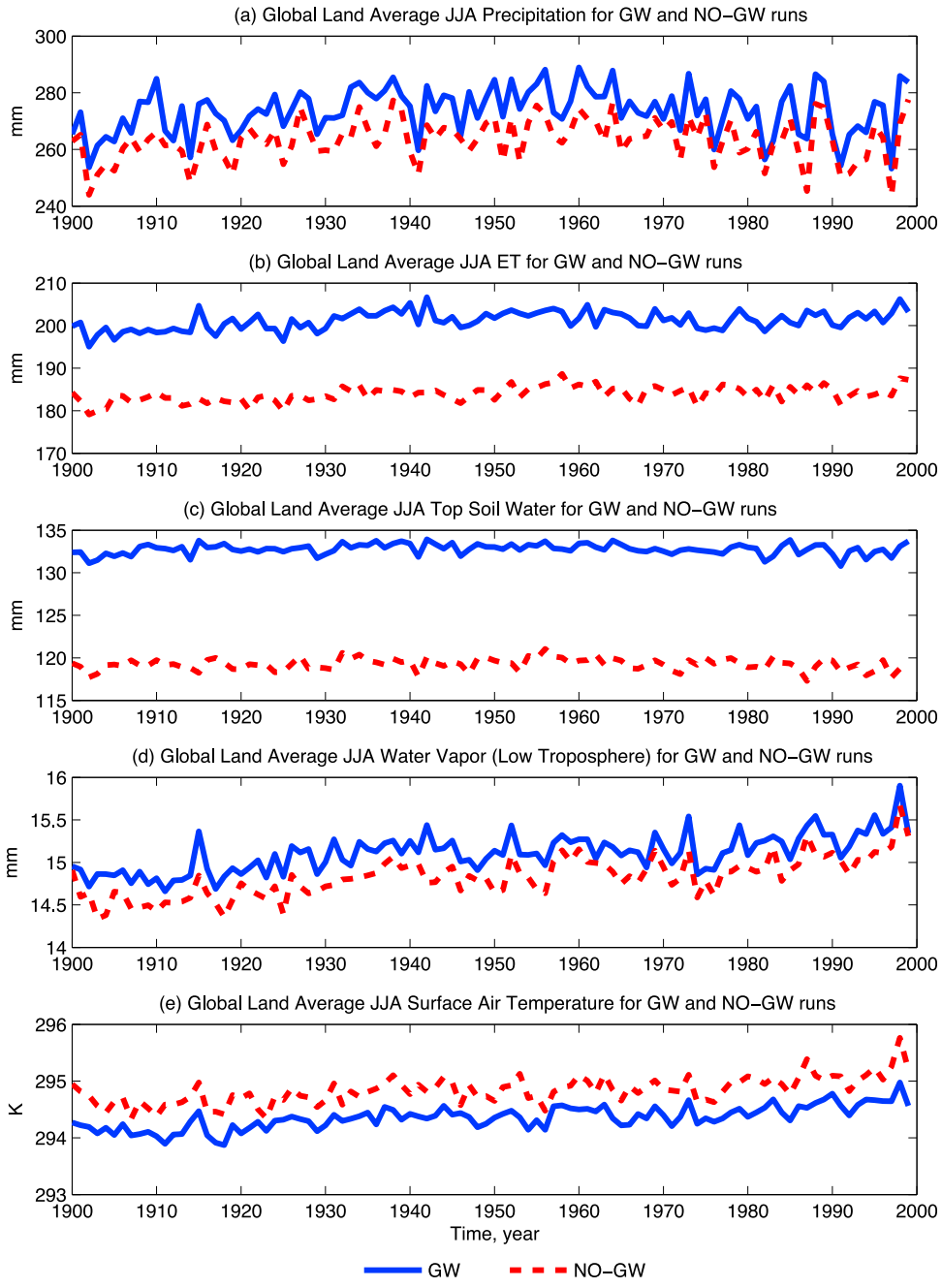

Figure 2. The global (−180°–180°, 60°S–60°N) land average of (a) precipitation, (b) evapotranspiration (ET), (c) top (~0–50 cm) soil water, (d) lower tropospheric (surface to 850 mbar) integrated water vapor, and (e) surface air temperature for the GW and NO-GW runs in June, July, and August (JJA) from 1900 to 1999.

where $(\,)'$ represents the anomalies (i.e., GW minus NO-GW) due to the impact of groundwater in the model.

[15] Therefore, P' shown in Figure 3a can be decomposed into ET', $-\langle \mathbf{v} \cdot \nabla q \rangle'$, and $-\left\langle w \frac{\partial q}{\partial p} \right\rangle'$ as shown in Figure 4 (all in energy units, $\frac{W}{m^2}$). The spatial distribution of $-\left\langle w \frac{\partial q}{\partial p} \right\rangle'$ is similar to precipitation anomalies in the tropics (Figures 4a and 4d), especially in the asymmetric dipoles over tropical land regions with the positive anomalies in the north and negative anomalies in the south along the equator. On the other hand, evapotranspiration (Figure 4b) is the major contributor to precipitation anomalies in the midlatitude of the Northern Hemisphere.

3.3. Precipitation Changes at the Equator

[16] The clear positive trend (with significance p-value less than 0.05) in Figure 3c indicates that the asymmetric response of precipitation is amplified with time near the equator. To explore what causes such amplifications, P' in Figure 3c is also decomposed to ET', $-\langle \mathbf{v} \cdot \nabla q \rangle'$, and

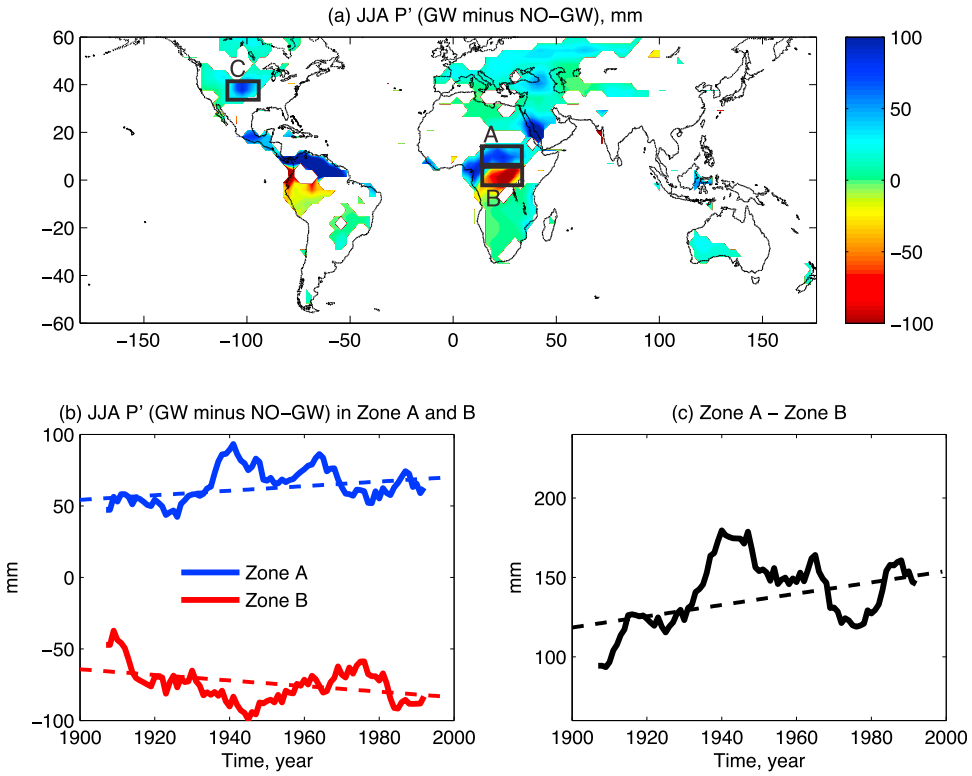

Figure 3. (a) The spatial pattern of the 100 year JJA composite for significant (p-value < 0.05) precipitation differences (GW minus NO-GW), (b) the 100 year time series (15 year running mean is applied) of averaged precipitation for the two black outlined boxes (Zone A and Zone B) in Figure 3a, and (c) the time series differences between Zone A and Zone B. Dashed line indicates the linear trend for the 100 year JJA time series.

$-\left\langle w\frac{\partial q}{\partial p}\right\rangle'$ on the basis of the moisture budget equation (equation (6)). Figures 5a–5d are the 100 year time series with a 15 year running mean applied, for P', ET', $-\langle \mathbf{v}\cdot\nabla q\rangle'$, and $-\left\langle w\frac{\partial q}{\partial p}\right\rangle'$, respectively. Figure 5 shows a similar pattern in the time series of $-\left\langle w\frac{\partial q}{\partial p}\right\rangle'$ and P', highlighting the importance of the contribution of $-\left\langle w\frac{\partial q}{\partial p}\right\rangle'$ to the precipitation responses. The more detailed features of their relationship can be seen in Figures 5e–5g, in which the difference (Zone A minus Zone B) of P' is plotted versus the differences of ET', $-\langle \mathbf{v}\cdot\nabla q\rangle'$, and $-\left\langle w\frac{\partial q}{\partial p}\right\rangle'$, respectively, for the 100 year time period. The results shown in Figure 5 reflect the major contribution of the $-\left\langle w\frac{\partial q}{\partial p}\right\rangle'$ term to the amplification of the asymmetric responses in precipitation. The $-\left\langle w\frac{\partial q}{\partial p}\right\rangle'$ term accounts for 71% of the variance (R^2 = 0.71) in the asymmetric precipitation responses, while the other two terms (ET' and $-\langle \mathbf{v}\cdot\nabla q\rangle'$) contribute less than 10%, hence, having little impact on the precipitation asymmetry over tropical land areas.

[17] The $-\left\langle w\frac{\partial q}{\partial p}\right\rangle'$ term depends on the redistribution of vertical atmospheric water vapor [*Chou et al.*, 2006]. The increase in water vapor in the lower troposphere induced by wetter soil in the GW run results in greater vertical moisture transport in the ascending branch of the Hadley circulation. This process enhances convection, causing more precipitation to occur over the regions where precipitation amounts are already climatological large [*Chou and Neelin*, 2004]. *Chou and Neelin* [2004] referred to this effect as the "rich-get-richer" mechanism, in which precipitation tends to increase more in convection zones and decrease more in subsidence zones under conditions of global warming. They showed that an increase in water vapor in the lower troposphere induced by global warming tended to increase tropical precipitation over regions where high levels of convection exist. These regions usually have a mean state of upward vertical velocity and high climatological precipitation.

[18] The Hadley circulation over land (Africa and South America) is shown in Figure 6, which also includes the zonally averaged mean pressure velocity (shading: dark gray indicates upward motion; light gray indicates downward motion) and anomalous pressure velocity (contours: negative upward). The vectors are anomalous winds (GW minus NO-GW) for the meridional components v' (m/s) and w' (hPa/s). As seen in Figure 6, upward velocity anomalies occur in the ascending branch of the Hadley circulation in the Northern Hemisphere during the summer. Owing to the anomalous upward velocity, anomalous downward motion near the southern margin of the ascending branch is formed

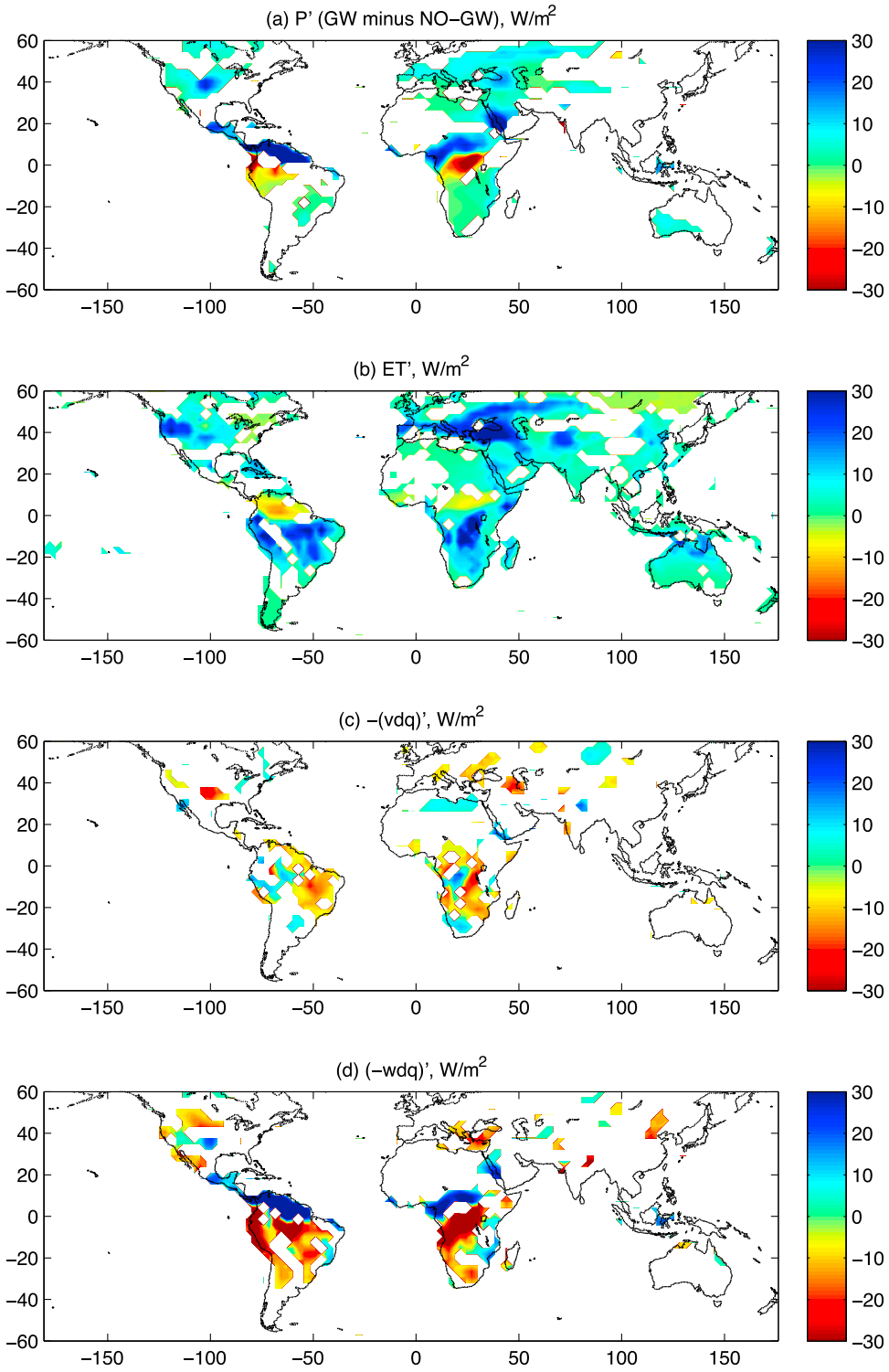

Figure 4. Spatial distributions of the four terms in equation (6) in JJA: (a) P', (b) ET', (c) $-\langle \mathbf{v} \cdot \nabla q \rangle'$, and (d) $-\left\langle w \frac{\partial q}{\partial p} \right\rangle'$. All the terms are in energy units of W/m^2. The white areas correspond to regions that are not significant at the 0.05 significance level.

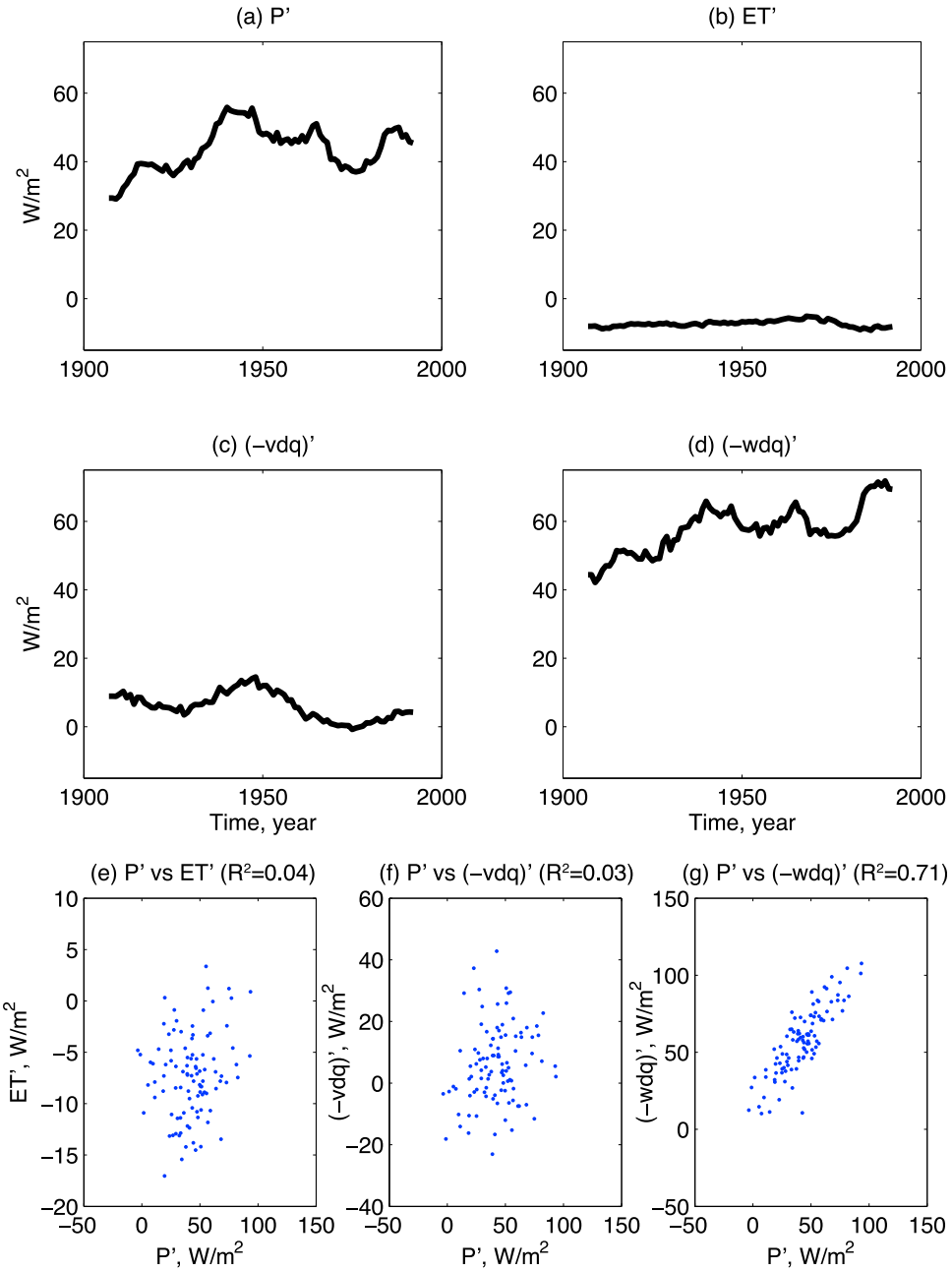

Figure 5. (a–d) The differences (Zone A minus Zone B) of 100 year time series of P', ET', $-\langle \mathbf{v} \cdot \nabla q \rangle'$, and $-\left\langle w \frac{\partial q}{\partial p} \right\rangle'$, respectively. A 15 year running mean is applied in the time series. (e–g) The difference of P' versus the differences of ET', $-\langle \mathbf{v} \cdot \nabla q \rangle'$, and $-\left\langle w \frac{\partial q}{\partial p} \right\rangle'$, respectively. Note that Figure 5a is the same as Figure 3c but in different units.

(as shown by the green wind vectors), resulting in decreased precipitation. This is consistent with the precipitation changes shown in Figure 3. Notice that in this study, we focus on the boreal summer precipitation changes; during the winter the asymmetric dipole near the equator still exists, but with opposite sign and smaller amplitude (results not shown here). Moreover, the increased precipitation over central North America is not observed during the winter season.

3.4. Precipitation Changes in Central North America

[19] While the $-\left\langle w \frac{\partial q}{\partial p} \right\rangle'$ contributes the most to the amplification of the asymmetric response over the equator, Figures 4a and 4b indicate that ET' may make some contributions to the precipitation anomalies in the midlatitudes of the Northern Hemisphere (e.g., central North America and eastern Europe). The 100 year time series of precipitation anomalies in central North America is examined in Figure 7 using the moisture budget equation. Figures 7a–7d

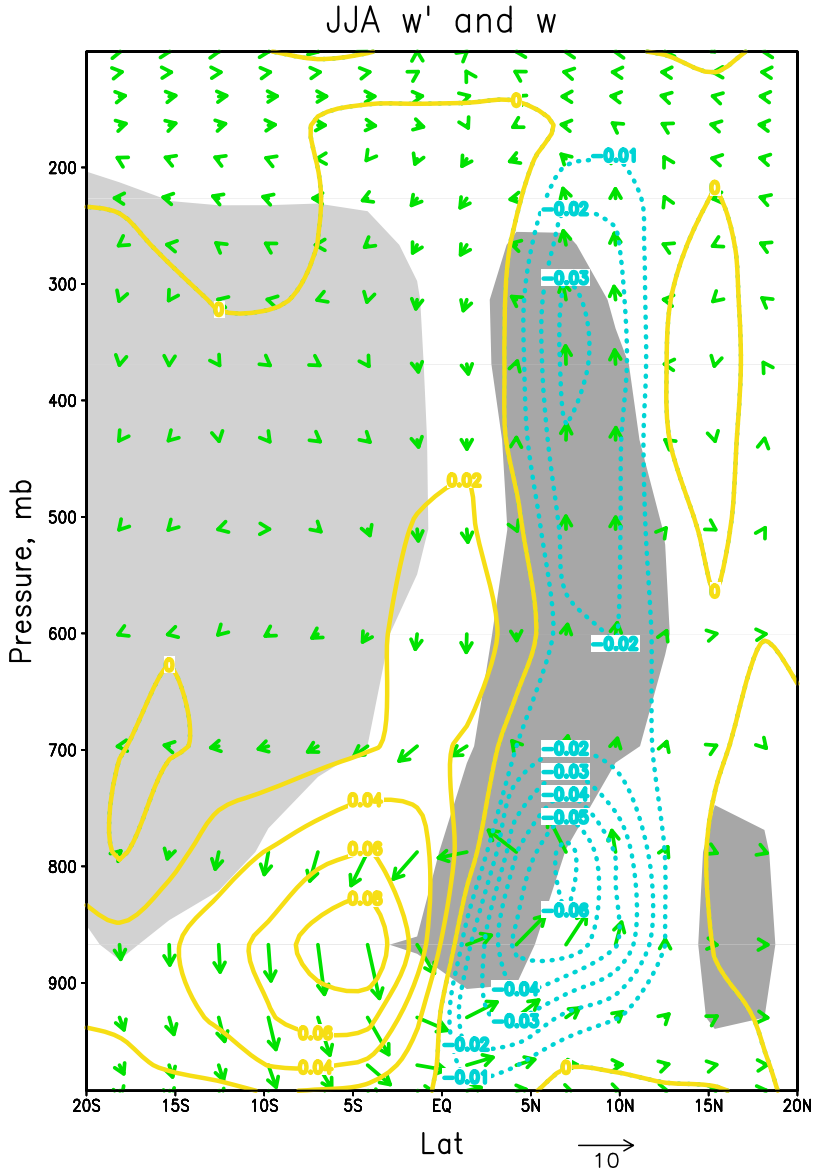

Figure 6. The zonally averaged mean pressure velocity (shading: dark gray indicates upward motion, and light gray indicates downward motion) and anomalous pressure velocity (contours: negative upward, hPa/s) during the summer. The vectors are anomalous winds (GW minus NO-GW) for the meridional components v' (m/s) and w' (hPa/s).

show the time series of the four terms of equation (6) for the black outlined box (Zone C) in Figure 3a. In this region, ET' has a very similar pattern to the precipitation anomaly (Figures 7a and 7b). Basically, ET' contributes about 60% of the variance (R^2 = 0.6) in the precipitation anomaly as shown in Figure 7e. Zone C is in fact located close to a "hot spot," defined by *Koster et al.* [2004] as a transition zone between wet and dry climates, where the atmosphere and land surface are strongly coupled. Hence, local evapotranspiration changes have a strong impact on precipitation anomalies. On the other hand, the precipitation anomalies in the tropical land regions are mainly controlled by vertical water vapor advection (or rather, the "rich-get-richer" mechanism).

[20] In central North America, since the average soil moisture content is below saturation, land evapotranspiration is more sensitive to soil water availability and thus exerts greater control on precipitation rates. In the tropics, where average levels of soil water content are much higher, the controlling process for precipitation will be more similar to those over the ocean (the large-scale circulation, i.e., Hadley Cell). This is the reason why the "rich-get-richer" mechanism can become a dominant factor. The relative magnitudes of ET' and $-\left\langle w\frac{\partial q}{\partial p}\right\rangle'$ in Figures 5 and 7 can demonstrate their importance to the two different mechanisms.

4. Positive Feedback of Land-Atmosphere Interactions

[21] An example of a simple positive feedback framework of land-atmosphere interactions can be explained as follows:

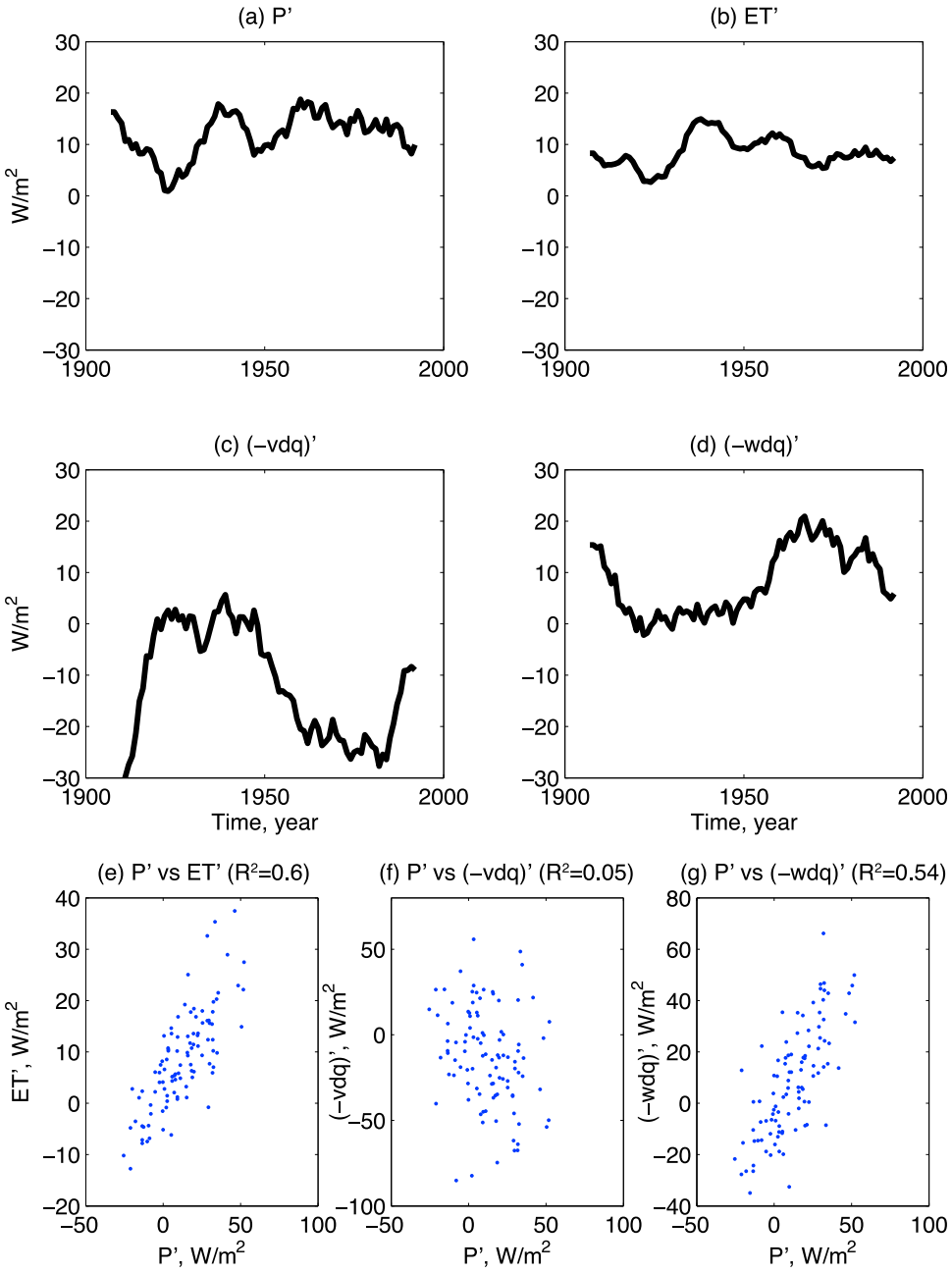

Figure 7. (a–d) The 100 year time series of P', ET', $-\langle \mathbf{v} \cdot \nabla q \rangle'$, and $-\left\langle w \frac{\partial q}{\partial p} \right\rangle'$ for Zone C of Figure 3a, respectively. A 15 year running mean is applied in the time series. (e–g) P' versus ET', $-\langle \mathbf{v} \cdot \nabla q \rangle'$, and $-\left\langle w \frac{\partial q}{\partial p} \right\rangle'$, respectively.

an increase in soil moisture levels can enhance evapotranspiration as well as water vapor of the lower troposphere, which in turn increase the precipitation rates that will then further moisten the soil. The cross-correlation coefficients between the anomalies of the four variables in the feedback loop (soil moisture, evapotranspiration, water vapor, and precipitation) are computed to explore whether this positive feedback exists. Figure 8 shows scatterplots of soil moisture versus evapotranspiration, evapotranspiration versus water vapor, water vapor versus precipitation, and precipitation versus soil moisture, respectively, for Zone A. In Figure 8, only precipitation and soil moisture anomalies show a strong correlation. This implies that the increased precipitation in this region does not follow the positive land-atmosphere feedback loop outlined above.

[22] Similarly, Figure 9 shows scatterplots of the same four variables for Zone C where ET' largely contributes to the precipitation anomaly as shown in Figure 7. High correlations are visible for each pair of the four variables, demonstrating a positive feedback of land-atmosphere

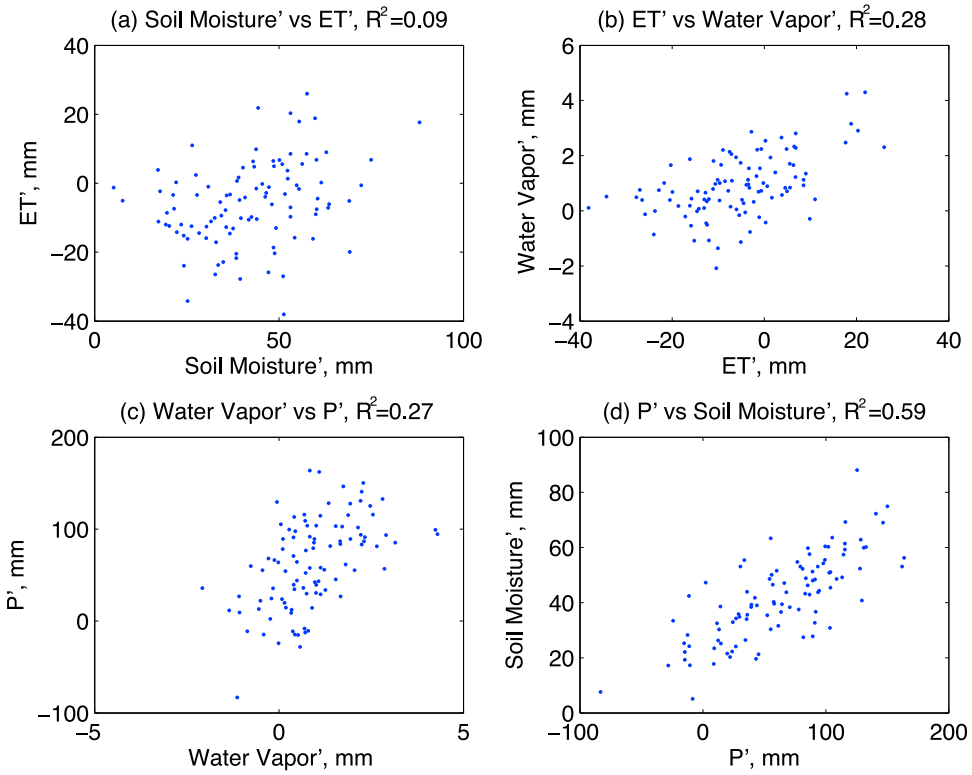

Figure 8. (a) Soil moisture versus evapotranspiration, (b) evapotranspiration versus water vapor, (c) water vapor versus precipitation, and (d) precipitation versus soil moisture for Zone A for 100 year simulations. All variables are anomalies (GW minus NO-GW).

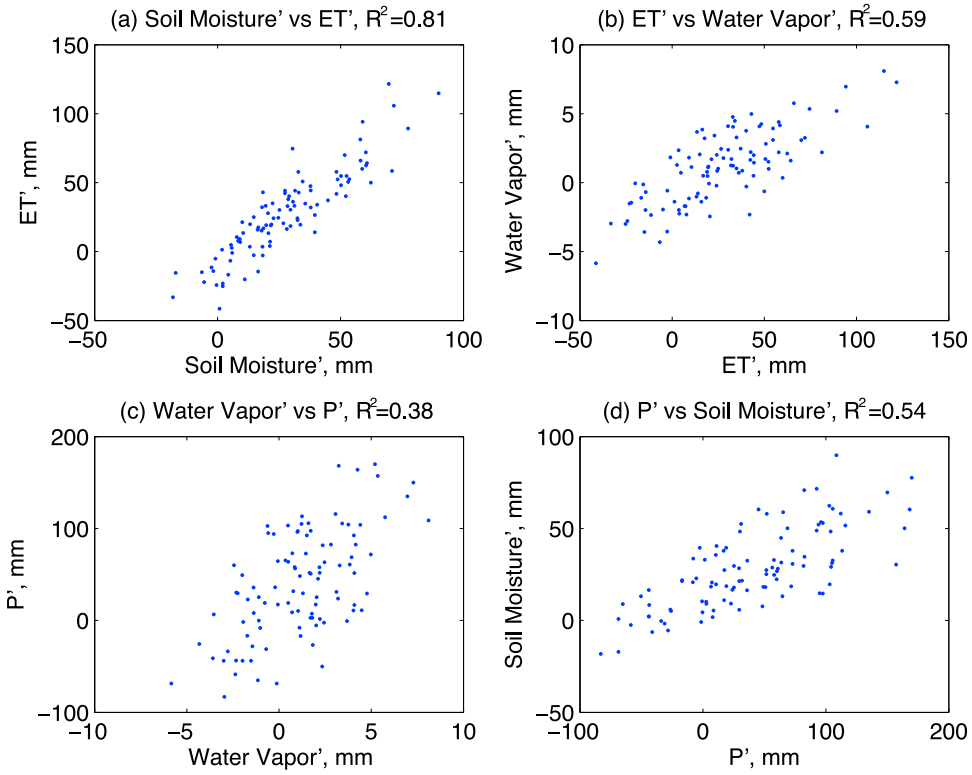

Figure 9. (a) Soil moisture versus evapotranspiration, (b) evapotranspiration versus water vapor, (c) water vapor versus precipitation, and (d) precipitation versus soil moisture for Zone C for 100 year simulations. All variables are anomalies (GW minus NO-GW).

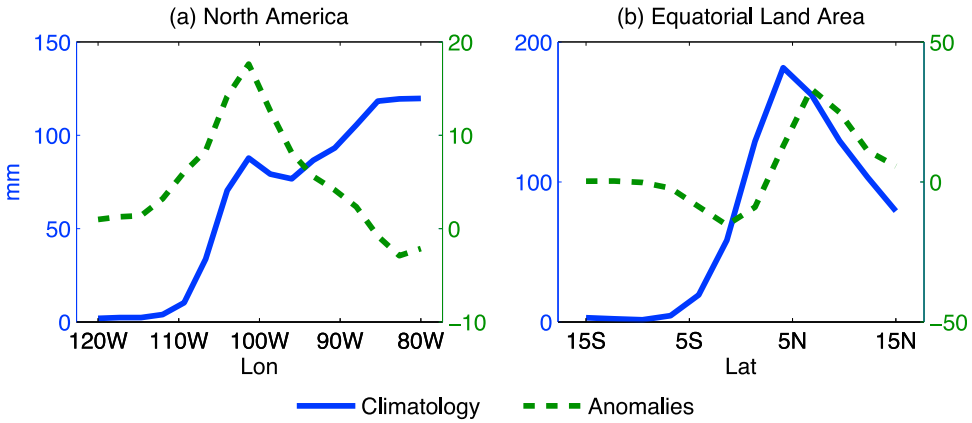

Figure 10. (a) The meridional average (30°N–42°N) of precipitation from 120°W to 80°W and (b) the zonal average over Africa and South America of precipitation from 15°S to 15°N for the JJA climatology (NO-GW run, blue line) and anomalies (GW minus NO-GW, green line) over the 100 year average.

interaction. Figures 8 and 9 support the idea that different mechanisms ("rich-get-richer" and positive feedback of land-atmosphere interaction) are responsible for the positive precipitation anomalies in Zones A and C, respectively. Moreover, results shown in Zone C are consistent with several recent studies [e.g., *Koster et al.*, 2004; *Anyah et al.*, 2008; *Yuan et al.*, 2008; *Jiang et al.*, 2009], which have indicated that land-atmosphere interactions are a critical mechanism for summer precipitation over the central U.S.

[23] Figure 10a shows the meridional average (30°N to 42°N) of precipitation from 120°W to 80°W for the JJA climatology (NO-GW run, blue line) and anomalies (GW minus NO-GW, green line) averaged over the 100 year time period. The precipitation climatology is lower in the west and progressively increases to the east. The higher precipitation anomalies can be seen over the transitional region (at around 100°W) where local evapotranspiration changes have a strong impact on precipitation anomalies, where a positive land-atmosphere feedback is active. On the other hand, Figure 10b is the zonal average of precipitation over land (Africa and South America), from 15°S to 15°N. It shows that both the higher climatology located over the Northern Hemisphere (at around 5°N) and the coincident location of the higher precipitation anomaly; that is the rich-get-richer. Figure 10 clearly shows the difference in impacts between the "rich-get-richer" and "positive land-atmosphere feedback" on precipitation changes due to groundwater.

[24] *Yeh et al.* [1984] and *Segal et al.* [1998] showed that regions with increased precipitation due to irrigation are highly dependent on the climatic regime. In arid zones (with descending motion), a significant amount of irrigated water will evaporate and be transported outside the irrigation region, therefore, having little effect on local precipitation. On the other hand, in wet zones (with ascending motion), precipitation can be greatly enhanced because of extra water vapor via irrigation. This is analogous to the "rich-get-richer" concept. This study demonstrates that groundwater has a similar effect (rich-get-richer) on the precipitation distributions over tropical land areas although the mechanism to moisten the soil is a bottom-up process.

5. Model Evaluations

[25] This section discusses whether the inclusion of capillary fluxes improves model simulations. We compare the spatial pattern of simulated precipitation to observations, and the time series climatology for four regions where significant differences of precipitation between the two runs exist. Figure 11a shows the spatial pattern of the 99 year (1901~1999) average JJA precipitation from the Climate Research Unit Time Series 2.1 (CRU) [*Mitchell and Jones*, 2005] data. Figures 11b and 11c are for the NO-GW and GW runs, respectively. Note that anomalously high precipitation is found in the Arabian Peninsula, a feature identified as a serious issue in CAM simulations by several studies [e.g., *Hack et al.*, 2006; *Wang et al.*, 2007; *Lawrence and Chase*, 2009]. This wet bias could be due to overestimated 850 mbar westerly winds over the Sahel, which results in anomalous low-level convergence and convection [*Levis et al.*, 2004]. The inclusion of capillary fluxes improves precipitation simulations in the wet areas of tropical land (region A and region D), but not for region B and region C, which can be seen from the climatology comparisons in Figures 11d–11g. Moreover, the sharp gradient between the wet and dry areas are noted in the observations, but not in the models. One possible reason is the coarse horizontal resolution used in the model, compared to the half-degree spatial resolution of the observations.

[26] Figure 12 compares simulated integrated low-level (surface to 700 mbar) water vapor for JJA climatology to that from NASA Water Vapor Project (NVAP) [*Randel et al.*, 1996]. For comparison to the NVAP data set, the JJA climatology for both the NVAP and model simulations were averaged from 1988 to 1999. Figure 12 shows that the model can capture the spatial variability of water vapor relatively well compared to that of precipitation, although the simulated water vapor shows less spatial variation. Figure 12 also indicates that water vapor in the Arabian

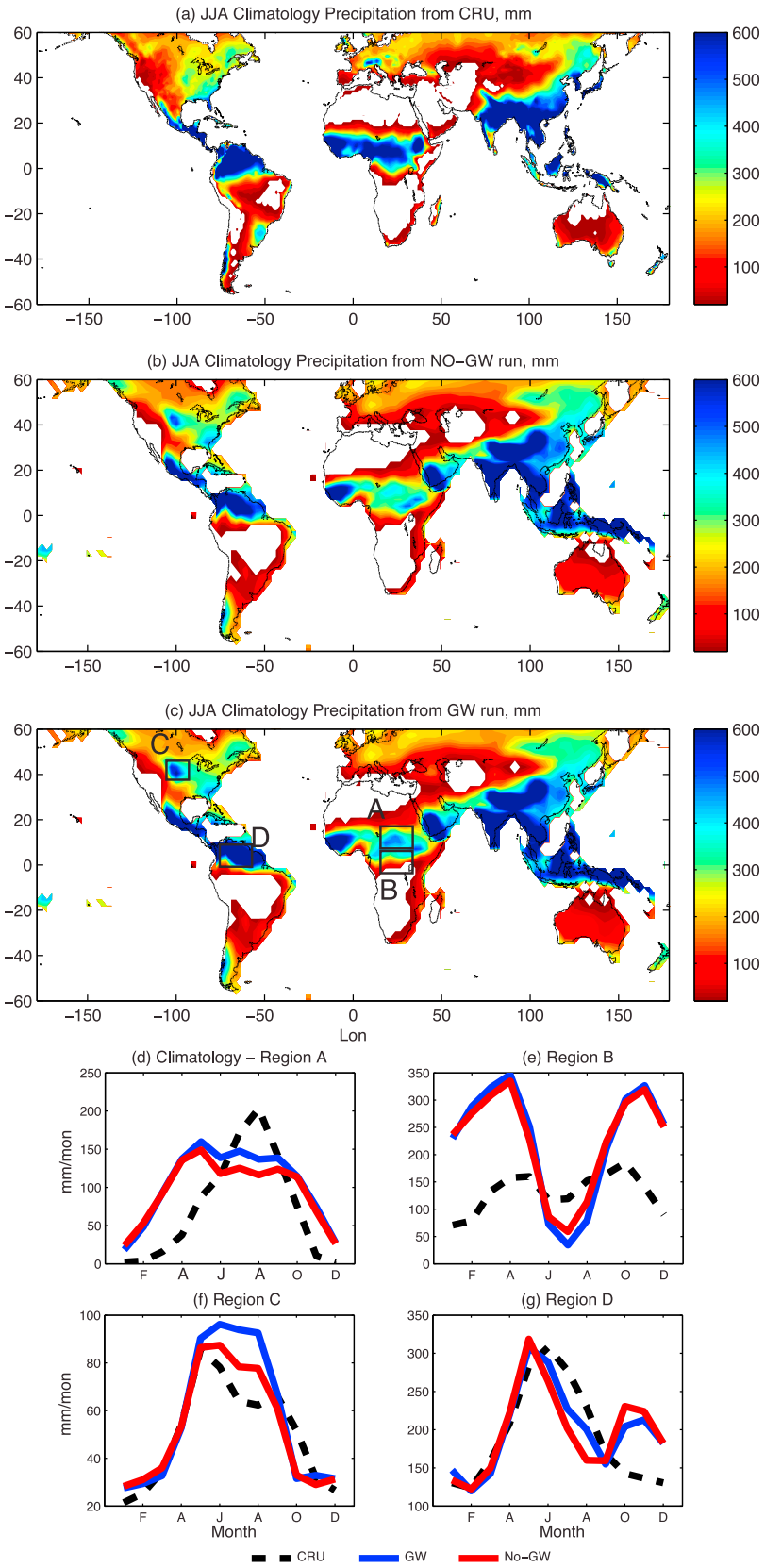

Figure 11. The spatial pattern of the 99 year (1901~1999) JJA precipitation composite for (a) the Climate Research Unit Time Series 2.1 (CRU), (b) NO-GW simulation, and (c) GW simulation. The white areas correspond to regions that are less than 20 mm. (d–g) The climatology comparison for the four black outlined boxes (Zones A–D in Figure 11c).

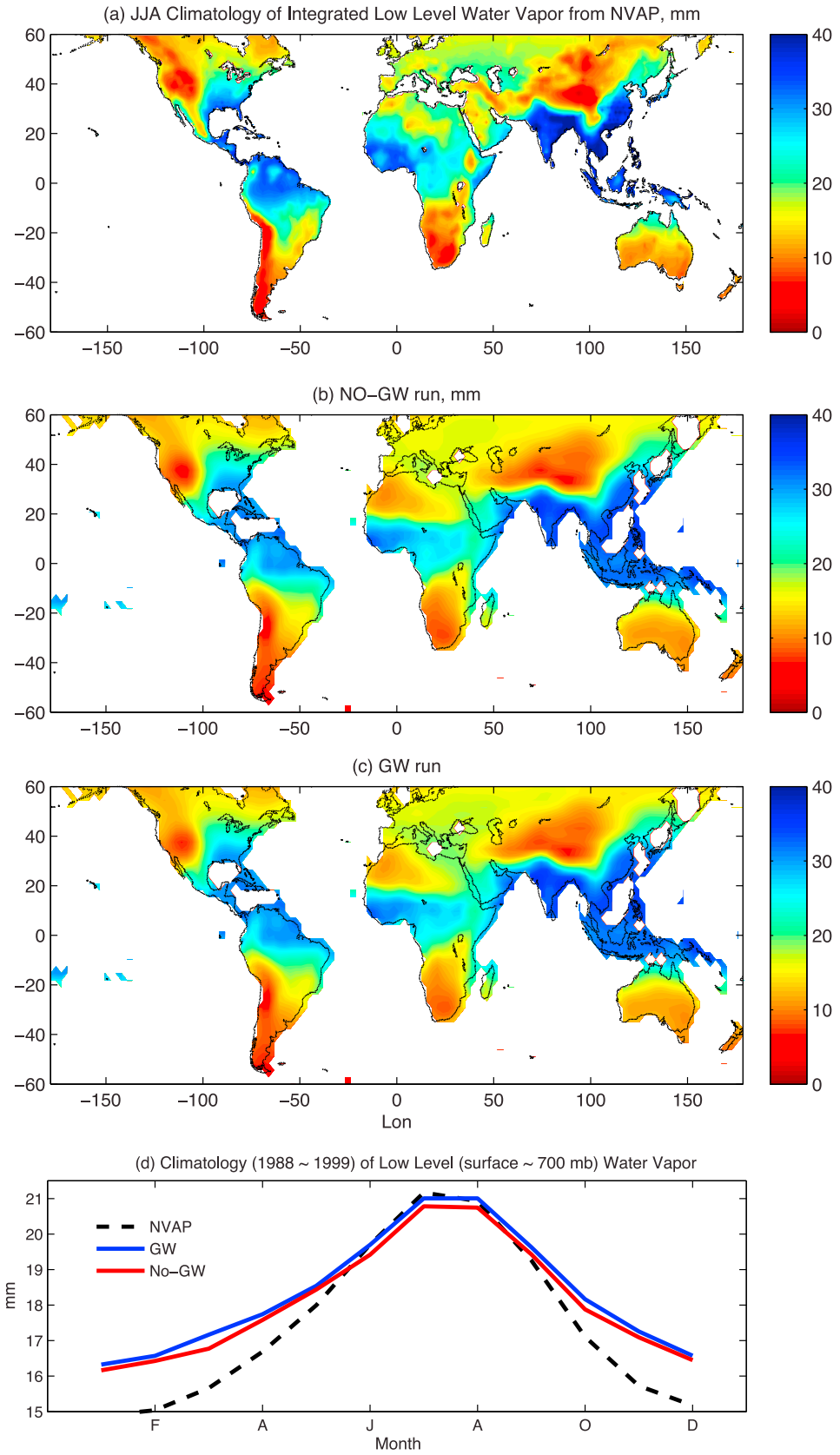

Figure 12. The spatial pattern of the 12 year (1988~1999) JJA low-level (from surface to 700 mbar) integrated water vapor composite for (a) NASA Water Vapor Project (NVAP), (b) NO-GW simulation, and (c) GW simulation. (d) The climatology of global land average for NVAP, the NO-GW run, and the GW run.

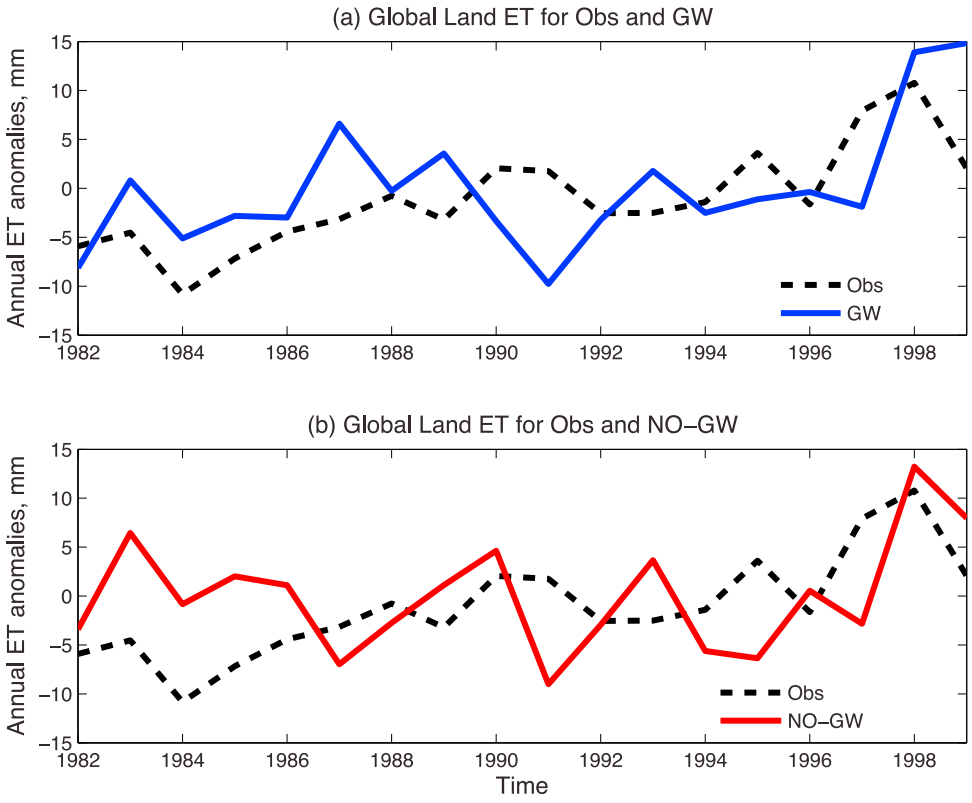

Figure 13. Global land ET anomaly comparisons from 1982 to 1999 for (a) the GW run and model tree ensemble (MTE) and (b) the NO-GW run and MTE.

Peninsula is overestimated, which is consistent with the wet bias shown in Figures 3 and 11. Figure 12d is the annual climatology comparison. The GW run has a better match with NVAP during the summer seasons compared to the NO-GW run; however, both runs overestimate the water vapor in other seasons.

[27] We also compare the time series anomalies of land-average evapotranspiration from model simulations to that of the model tree ensemble (MTE) product of *Jung et al.* [2010]. As can be seen in Figure 13, the two runs do not show significant differences; however, the slightly increasing trend shown in the MTE evapotranspiration can be captured better in the case of GW run than that of NO-GW run. This is due to the additional water supply from the groundwater aquifer resulting in an overall increase of ET as shown in Figure 2 and Table 1. Table 1 is a summary of simulated global average ET and precipitation compared to that from *Oki and Kanae* [2006]. The average precipitation over land slightly increases in the GW run compared to the NO-GW run; however, it is 15,700 km^3/yr (14%) higher than the value of *Oki and Kanae* [2006]. The average ET over land in both runs is higher to the value of *Oki and Kanae* [2006]. The simulated precipitation and ET are both overestimated in the oceans and in land while compared to *Oki and Kanae* [2006].

[28] Figures 11–13 indicate that an inclusion of groundwater does not always improve GCM simulations. This could be due to the globally constant groundwater parameters or the lack of groundwater lateral flow and human groundwater withdrawal in the model. This also indicates the importance of applying a more realistic groundwater model in the GCM. Other factors, such as air-sea interactions, aerosol-cloud interaction, and the human water management practices could have significant impacts on model simulations, which also need to be carefully addressed.

[29] Figure 14 shows the average water table depth and runoff from 1900~1999 for the GW run. Note that this model does not consider lateral groundwater flow, so the spatial pattern of water table depth closely follows the climate-driven precipitation pattern. When compared to the results shown in Figure 2 of *Niu et al.* [2007], simulated water table depth and runoff capture the major spatial patterns, for example, the deep water table in the western U.S., the Sahara desert, northern China, and the Middle East, in which the runoff simulations are relatively low. In regions, such as the eastern U.S., the Amazon and Congo basins, the water table is shallow with higher runoff. Owing to over-

Table 1. Comparison of Mean Annual Precipitation and Evapotranspiration for Averaged Land and Ocean From *Oki and Kanae* [2006], the GW Run, and the NO-GW Run[a]

	Oki and Kanae [2006]	CAM3.5 GW[b]	CAM3.5 NO-GW[b]
Precipitation/land	111	126.7	123.4
Precipitation/ocean	391	395.8	392.3
ET over land	65.5	81.3	74.6
E over ocean	436.5	443.4	443.3

[a]Units are 10^3 km^3/yr. CAM3.5, NCAR Community Atmosphere Model, version 3.5; GW, groundwater run; NO-GW, no groundwater run.
[b]The value of model simulations is the average from 100 years (1900–1999).

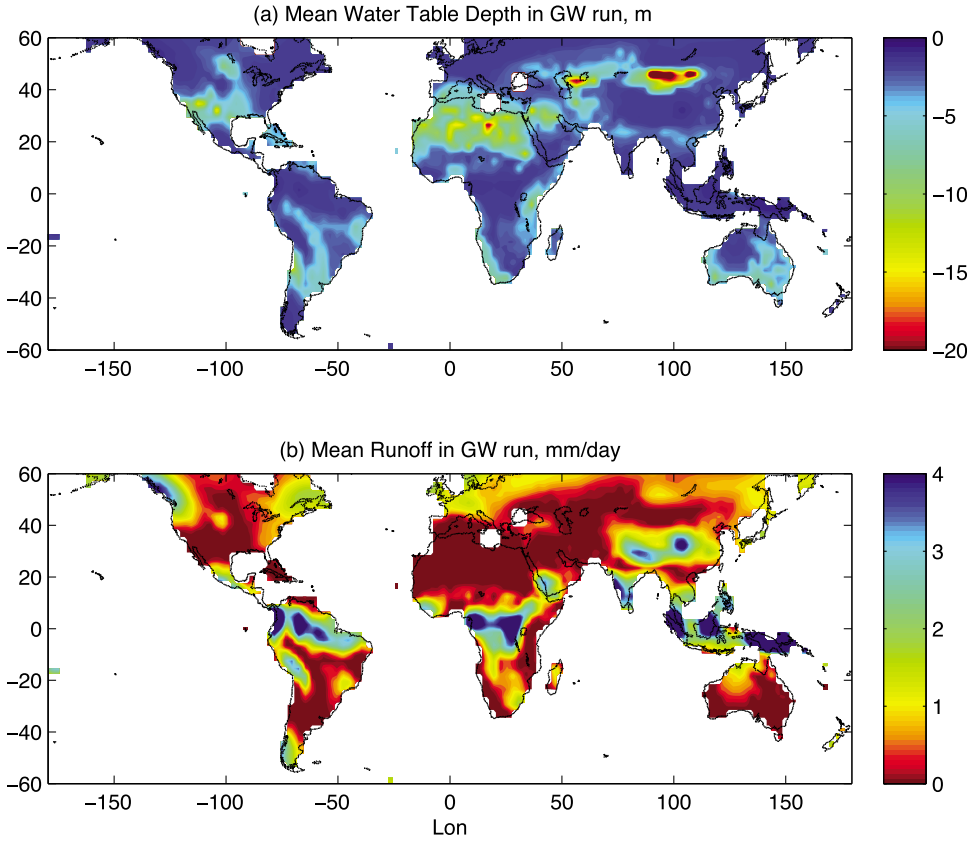

Figure 14. The spatial pattern of the (a) modeled 1900~1999 averaged water table depth and (b) modeled 1900~1999 averaged runoff in the GW run.

estimated precipitation in the Arabian Peninsula in CAM3.5, the simulated water table depth and runoff also have biases.

6. Discussion

[30] Cross-correlation analysis is used to explore the strength of land-atmosphere interactions. This analysis quantifies the first-order strength of land-atmosphere interactions; however, it is unable to actually distinguish between cause and effect. Two kinds of online experiments [e.g., *Chou et al.*, 2001] are suggested to further identify those relationships, that is, prescribed and interactive. For example, in a prescribed soil moisture experiment, soil moisture will be forced to maintain the climatology of observations, and surface temperature will be calculated from the surface heat flux budget. For an interactive soil moisture experiment, land subsurface hydrology (e.g., interactive soil moisture and groundwater) will be active, so that land surface fluxes are not only balanced in the heat budget but also in the water budget. These experiments (prescribed and interactive) are different from those in this study, in which the soil moisture or water table is not fixed.

[31] Moreover, the SIMTOP runoff model [*Niu et al.*, 2005] modified from TOPMODEL concept [e.g., *Beven and Kirkby*, 1979; *Famiglietti and Wood*, 1994] is applied for surface and subsurface runoff generation in the CLM3.5. However, evapotranspiration from saturated surface areas (e.g., where groundwater table reaches the land surface) or directly from groundwater aquifer via plants is not considered in the model thus far. Some studies [e.g., *Yeh and Famiglietti*, 2009] report that a significant contribution of groundwater to evapotranspiration can be observed in shallow water table areas. Consideration of such evapotranspiration processes could further enhance the precipitation asymmetric response since more water vapor could be transported from land to the atmosphere. In addition, this study uses the equilibrium water table depth proposed by *Lo and Famiglietti* [2010] as the initial condition. However, how water table variations affect the asymmetric response of precipitation over the equator or the positive precipitation anomaly in the "hot spot" or, to what extent the depth of the water table affects the precipitation distributions; for example, if water table depths are held constant in time, will the asymmetric responses of precipitation still exist? Additional experiments and study will be required.

[32] The "rich-get-richer" mechanism proposed by *Chou and Neelin* [2004] is based on a global warming scenario, in which the entire troposphere warms up and convection can be affected through the surface to the upper troposphere (200 mbar) [*Chou et al.*, 2009]. However, in this study, all changes start from the bottom (groundwater) to affect the lower troposphere through evapotranspiration. Convection anomalies for the tropics (green wind vectors in Figure 6) are confined in the lower troposphere (below 700 mbar). As discussed above, the impact of groundwater on the precip-

itation response can be enhanced if other evapotranspiration processes are included in the model; hence, it may show the impacts of groundwater higher in the troposphere. Furthermore, the $-\left\langle w\frac{\partial q}{\partial p}\right\rangle'$ term can be divided into thermodynamic (change in q, i.e., $-\left\langle \overline{w}\left(\frac{\partial q}{\partial p}\right)'\right\rangle$) and dynamic components (change in w, i.e., $-\left\langle w'\left(\frac{\partial \overline{q}}{\partial p}\right)\right\rangle$). On the basis of the work of *Chou et al.* [2009], the thermodynamic component is the relatively easy part to simulate, but the dynamic component is more complicated and difficult to simulate consistently among models. Here, we do not perform such analyses since our focus is on the relative magnitude of the ET' and $-\left\langle w\frac{\partial q}{\partial p}\right\rangle'$ terms of the moisture budget equation for the global distribution. Such subcomponent analyses in the moisture budget equation will be an important future step in order to better understand how the "rich-get-richer" mechanism is represented in models. In addition, GCM experiments [*Cook and Ganadeskian*, 1991; *Xue and Shukla*, 1993] have shown that tropical convection may shift in response to altered soil moisture conditions. In this study, however, the shift of convection in the tropics was not significant (Figure 10b), likely owing to the coarse model resolution of the simulations.

7. Conclusions

[33] Spatial variations in precipitation response to groundwater are evaluated in coupled land-atmosphere climate model simulations. Results show that the effect of groundwater on the amount of precipitation is not globally homogeneous. In the boreal summer, tropical land regions show a positive anomaly in the Northern Hemisphere, and a negative anomaly in the Southern Hemisphere. Increased precipitation essentially follows the climatology of the convective zone. As a result, an asymmetric dipole is found over tropical land regions along the equator. A moisture budget analysis reveals that the vertical moisture advection term is the main contributor to the asymmetric dipole of precipitation anomalies in central Africa along the equator. With a groundwater representation in the model, water vapor in the lower troposphere increases. The Hadley circulation transports more water vapor upward causing a positive precipitation anomaly in the ascending branch; that is, the "rich-get-richer" mechanism. Hence, water vapor in the descending branch of the Hadley circulation is reduced by a strengthened downward motion, which results in a decline of precipitation.

[34] The "rich-get-richer" mechanism does not apply to the precipitation anomaly in the transitional climatic zone of central North America. In fact, this region experiences a positive feedback loop of land-atmosphere interaction. When soil moisture is high owing to presence of groundwater in the model, more moisture will be transported vertically from the land to the atmosphere via evapotranspiration. With an increase in atmospheric moisture, convection can be triggered relatively easily, resulting in more precipitation. A positive feedback loop develops in which wet soil moisture conditions lead to more precipitation, and more precipitation sustains the wet soil moisture conditions. This positive feedback is usually observed in regions with high levels of interaction between the land and atmosphere. Such regions are usually located close to a "hot spot," defined by *Koster et al.* [2004] as a transition zone between wet and dry climates, where the atmosphere and land surface are strongly coupled.

[35] The "rich-get-richer" and regional positive land-atmosphere feedback are two completely different mechanisms responsible for the spatial variation of precipitation caused by groundwater in tropical land regions and central North America, respectively. These findings are consistent with previous studies [e.g., *Anyah et al.*, 2008], which reported that impacts of groundwater on the precipitation are highly spatially varied. In fact, several studies [e.g., *Famiglietti and Wood*, 1994, 1995; *Anyah et al.*, 2008; *Kollet and Maxwell*, 2008] have reported on the nonlinear relationships between the soil moisture and water table depth and other hydrologic fluxes (e.g., runoff and evapotranspiration). Moreover, this study shows that wet areas may get wetter and dry areas may get drier in tropical land regions after incorporating capillary rise from groundwater. Analyses from IPCC fourth Assessment Report (AR4) model simulations [e.g., *Sun et al.*, 2007] have shown that under global warming, extreme climatic events (droughts and floods) are expected to increase. Most of the IPCC AR4 models, however, lack any representation of groundwater aquifers. This work suggests that after incorporating a groundwater component into the IPCC GCMs, that extreme events may further increase, or conversely, that current predictions underestimate potential increases in hydrologic extremes. Finally, precipitation, a critical component of the global water cycle, is not well represented in GCMs. This study indicates that an inclusion of simple groundwater parameterization does not always improve precipitation simulations. A better representation of subsurface land hydrology and more realistic groundwater model in GCMs are necessary to better simulate global precipitation processes.

[36] **Acknowledgments.** This research was sponsored by NOAA CPPA grant NA05OAR4310013 and the NASA Earth and Space Science Fellowship program NNX08AV06H. We express our gratitude to Chia Chou for valuable feedback.

References

Amenu, G. G., P. Kumar, and X. Z. Liang (2005), Interannual variability of deep-layer hydrologic memory and mechanisms of its influence on surface energy fluxes, *J. Clim.*, *18*, 5024–5045, doi:10.1175/JCLI3590.1.

Anyah, R. O., C. P. Weaver, G. Miguez-Macho, Y. Fan, and A. Robock (2008), Incorporating water table dynamics in climate modeling: 3. Simulated groundwater influence on coupled land-atmosphere variability, *J. Geophys. Res.*, *113*, D07103, doi:10.1029/2007JD009087.

Beven, K. J., and M. J. Kirkby (1979), A physically based, variable contributing model of basin hydrology, *Hydrol. Sci. Bull.*, *24*, 43–69, doi:10.1080/02626667909491834.

Brooks, R. H., and A. T. Corey (1964), Hydraulic properties of porous media, *Hydrol. Pap. 3*, Colo. State Univ., Fort Collins.

Chen, X., and Q. Hu (2004), Groundwater influences on soil moisture and surface evaporation, *J. Hydrol. Amsterdam*, *297*, 285–300, doi:10.1016/j.jhydrol.2004.04.019.

Chou, C., and J. D. Neelin (2004), Mechanisms of global warming impacts on regional tropical precipitation, *J. Clim.*, *17*, 2688–2701, doi:10.1175/1520-0442(2004)017<2688:MOGWIO>2.0.CO;2.

Chou, C., J. D. Neelin, and H. Su (2001), Ocean-atmosphere-land feedbacks in an idealized monsoon, *Q. J. R. Meteorol. Soc.*, *127*, 1869–1891, doi:10.1002/qj.49712757602.

Chou, C., J. D. Neelin, J.-Y. Tu, and C.-T. Chen (2006), Regional tropical precipitation change mechanisms in ECHAM4/OPYC3 under global warming, *J. Clim.*, *19*, 4207–4223, doi:10.1175/JCLI3858.1.

Chou, C., J. D. Neelin, C.-A. Chen, and J.-Y. Tu (2009), Evaluating the "rich-get-richer" mechanism in tropical precipitation change under global warming, *J. Clim.*, *22*, 1982–2005, doi:10.1175/2008JCLI2471.1.

Cook, K. H., and A. Ganadeskian (1991), Effects of saturated and dry land surfaces on tropical circulation and precipitation in a general circulation model, *J. Clim.*, *4*, 873–889, doi:10.1175/1520-0442(1991)004<0873:EOSADL>2.0.CO;2.

Delworth, T., and S. Manabe (1993), Climate variability and land-surface processes, *Adv. Water Resour.*, *16*, 3–20, doi:10.1016/0309-1708(93)90026-C.

Dickinson, R. E., A. Henderson-Sellers, P. J. Kennedy, and M. F. Wilson (1986), Biosphere-Atmosphere Transfer Scheme (BATS) for the NCAR CCM, *Tech. Note NCAR/TN-275-STR*, Natl. Cent. for Atmos. Res., Boulder, Colo.

Dirmeyer, P. A. (2001), An evaluation of the strength of land-atmosphere coupling, *J. Hydrometeorol.*, *2*, 329–344, doi:10.1175/1525-7541(2001)002<0329:AEOTSO>2.0.CO;2.

D'Odorico, P., and A. Porporato (2004), Preferential states in soil moisture and climate dynamics, *Proc. Natl. Acad. Sci. U. S. A.*, *101*, 8848–8851, doi:10.1073/pnas.0401428101.

Elmore, A. J., J. M. Kaste, G. S. Okin, and M. S. Fantle (2008), Groundwater influences on atmospheric dust generation in deserts, *J. Arid Environ.*, *72*(10), 1753–1765, doi:10.1016/j.jaridenv.2008.05.008.

Eltahir, E. A. B. (1998), A soil moisture rainfall feedback mechanism: 1. Theory and observations, *Water Resour. Res.*, *34*, 765–776, doi:10.1029/97WR03499.

Entekhabi, D., and P. Eagleson (1989), Land surface hydrology parameterization for atmospheric general circulation models including subgrid scale spatial variability, *J. Clim.*, *2*, 816–831, doi:10.1175/1520-0442(1989)002<0816:LSHPFA>2.0.CO;2.

Famiglietti, J. S., and E. F. Wood (1991), Evapotranspiration and runoff from large land areas: Land surface hydrology for atmospheric general circulation models, *Surv. Geophys.*, *12*, 179–204, doi:10.1007/BF01903418.

Famiglietti, J. S., and E. F. Wood (1994), Multi-scale modeling of spatially variable water and energy balance processes, *Water Resour. Res.*, *30*, 3061–3078, doi:10.1029/94WR01498.

Famiglietti, J. S., and E. F. Wood (1995), Effects of spatial variability and scale on areally averaged evapotranspiration, *Water Resour. Res.*, *31*, 699–712, doi:10.1029/94WR02820.

Fan, Y., G. Miguez-Macho, C. Weaver, R. Walko, and A. Robock (2007), Incorporating water table dynamics in climate modeling: 1. Water table observations and the equilibrium water table, *J. Geophys. Res.*, *112*, D10125, doi:10.1029/2006JD008111.

Findell, K. L., and E. A. B. Eltahir (1997), An analysis of the soil moisture-rainfall feedback, based on direct observations from Illinois, *Water Resour. Res.*, *33*, 725–735, doi:10.1029/96WR03756.

Gent, P. R., S. G. Yeager, R. B. Neale, S. Levis, and D. A. Bailey (2009), Improvements in a half degree atmosphere/land version of the CCSM, *Clim. Dyn.*, *34*, 819–833, doi:10.1007/s00382-009-0614-8.

Güntner, A., J. Stuck, S. Werth, P. Döll, K. Verzano, and B. Merz (2007), A global analysis of temporal and spatial variations in continental water storage, *Water Resour. Res.*, *43*, W05416, doi:10.1029/2006WR005247.

Gutowski, W. J., et al. (2002), A Coupled Land-Atmosphere Simulation Program (CLASP): Calibration and validation, *J. Geophys. Res.*, *107*(D16), 4283, doi:10.1029/2001JD000392.

Hack, J. J., J. M. Caron, S. G. Yeager, K. W. Oleson, M. M. Holland, J. E. Truesdale, and P. J. Rasch (2006), Simulation of the global hydrological cycle in the CCSM Community Atmosphere Model Version 3 (CAM3): Mean features, *J. Clim.*, *19*, 2199–2221, doi:10.1175/JCLI3755.1.

Hurrell, J. W., et al. (2008), A new sea surface temperature and sea ice boundary dataset for the community atmosphere model, *J. Clim.*, *21*, 5145–5153, doi:10.1175/2008JCLI2292.1.

Jiang, X., G.-Y. Niu, and Z.-L. Yang (2009), Impacts of vegetation and groundwater dynamics on warm season precipitation over the Central United States, *J. Geophys. Res.*, *114*, D06109, doi:10.1029/2008JD010756.

Jung, M., et al. (2010), Recent decline in the global land evapotranspiration trend due to limited moisture supply, *Nature*, *467*, 951–954, doi:10.1038/nature09396.

Kollet, S. J., and R. M. Maxwell (2008), Capturing the influence of groundwater dynamics on land surface processes using an integrated, distributed watershed model, *Water Resour. Res.*, *44*, W02402, doi:10.1029/2007WR006004.

Koster, R. D., and M. J. Suarez (2001), Soil moisture memory in climate models, *J. Hydrometeorol.*, *2*, 558–570, doi:10.1175/1525-7541(2001)002<0558:SMMICM>2.0.CO;2.

Koster, R. D., and M. J. Suarez (2003), Impact of land surface initialization on seasonal precipitation and temperature prediction, *J. Hydrometeorol.*, *4*, 408–423, doi:10.1175/1525-7541(2003)4<408:IOLSIO>2.0.CO;2.

Koster, R. D., M. J. Suarez, and M. Heiser (2000), Variance and predictability of precipitation at seasonal-to-interannual timescales, *J. Hydrometeorol.*, *1*, 26–46, doi:10.1175/1525-7541(2000)001<0026:VAPOPA>2.0.CO;2.

Koster, R. D., M. J. Suarez, R. W. Higgins, and H. M. Van den Dool (2003), Observational evidence that soil moisture variations affect precipitation, *Geophys. Res. Lett.*, *30*(5), 1241, doi:10.1029/2002GL016571.

Koster, R. D., et al. (2004), Regions of strong coupling between soil moisture and precipitation, *Science*, *305*, 1138–1140, doi:10.1126/science.1100217.

Koutsoyiannis, D., A. Efstratiadis, and K. Georgakakos (2007), Uncertainty assessment of future hydroclimatic predictions: A comparison of probabilistic and scenario-based approaches, *J. Hydrometeorol.*, *8*, 261–281, doi:10.1175/JHM576.1.

Lawrence, P. J., and T. N. Chase (2009), Climate impacts of making evapotranspiration in the Community Land Model (CLM3) consistent with the Simple Biosphere Model (SiB), *J. Hydrometeorol.*, *10*, 374–394, doi:10.1175/2008JHM987.1.

Levis, S., G. B. Bonan, and C. Bonfils (2004), Soil feedback drives the mid-Holocene North African monsoon northward in fully coupled CCSM2 simulations with a dynamic vegetation model, *Clim. Dyn.*, *23*, 791–802, doi:10.1007/s00382-004-0477-y.

Liang, X., Z. Xie, and M. Huang (2003), A new parameterization for surface and groundwater interactions and its impact on water budgets with the variable infiltration capacity (VIC) land surface model, *J. Geophys. Res.*, *108*(D16), 8613, doi:10.1029/2002JD003090.

Lo, M.-H., and J. S. Famiglietti (2010), Effect of water table dynamics on land surface hydrologic memory, *J. Geophys. Res.*, *115*, D22118, doi:10.1029/2010JD014191.

Lo, M.-H., P. J.-F. Yeh, and J. S. Famiglietti (2008), Constraining water table depth simulations in a land surface model using estimated baseflow, *Adv. Water Resour.*, *31*, 1552–1564, doi:10.1016/j.advwatres.2008.06.007.

Manabe, S. (1969), Climate and the ocean circulation: 1, The atmospheric circulation and the hydrology of the Earth's surface, *Mon. Weather Rev.*, *97*, 739–805, doi:10.1175/1520-0493(1969)097<0739:CATOC>2.3.CO;2.

Maxwell, R. M., and N. L. Miller (2005), Development of a coupled land surface and groundwater model, *J. Hydrometeorol.*, *6*, 233–247, doi:10.1175/JHM422.1.

Maxwell, R. M., F. K. Chow, and S. J. Kollet (2007), The groundwater land-surface-atmosphere connection: Soil moisture effects on the atmospheric boundary layer in fully coupled simulations, *Adv. Water Resour.*, *30*, 2447–2466, doi:10.1016/j.advwatres.2007.05.018.

Miguez-Macho, G., Y. Fan, C. P. Weaver, R. Walko, and A. Robock (2007), Incorporating water table dynamics in climate modeling: 2. Formulation, validation, and simulations of soil moisture fields, *J. Geophys. Res.*, *112*, D13108, doi:10.1029/2006JD008112.

Miguez-Macho, G., H. Li, and Y. Fan (2008), Simulated water table and soil moisture climatology over North America: Does the water table matter?, *Bull. Am. Meteorol. Soc.*, *89*, 663–672, doi:10.1175/BAMS-89-5-663.

Mitchell, T. D., and P. D. Jones (2005), An improved method of constructing a database of monthly climate observations and associated high-resolution grids, *Int. J. Climatol.*, *25*, 693–712, doi:10.1002/joc.1181.

Niu, G.-Y., Z.-L. Yang, R. E. Dickinson, and L. E. Gulden (2005), A simple TOPMODEL-based runoff parameterization (SIMTOP) for use in global climate models, *J. Geophys. Res.*, *110*, D21106, doi:10.1029/2005JD006111.

Niu, G.-Y., Z.-L. Yang, R. E. Dickinson, L. E. Gulden, and H. Su (2007), Development of a simple groundwater model for use in climate models and evaluation with Gravity Recovery and Climate Experiment data, *J. Geophys. Res.*, *112*, D07103, doi:10.1029/2006JD007522.

Oki, T., and S. Kanae (2006), Global hydrological cycles and world water resources, *Science*, *313*, 1068–1072, doi:10.1126/science.1128845.

Oleson, K. W., et al. (2008), Improvements to the Community Land Model and their impact on the hydrological cycle, *J. Geophys. Res.*, *113*, G01021, doi:10.1029/2007JG000563.

Quinn, P., K. Beven, and A. Culf (1995), The introduction of macroscale hydrological complexity into land surface–atmosphere transfer models and the effect on the planetary boundary layer development, *J. Hydrol. Amsterdam*, *166*, 421–444, doi:10.1016/0022-1694(94)05090-K.

Randel, D. L., T. H. Vonder Haar, M. A. Ringerud, G. L. Stephens, T. J. Greenwald, and C. L. Combs (1996), A new global water vapor dataset, *Bull. Am. Meteorol. Soc.*, *77*, 1233–1246, doi:10.1175/1520-0477(1996)077<1233:ANGWVD>2.0.CO;2.

Segal, M., Z. Pan, R. W. Turner, and E. S. Takle (1998), On the potential impact of irrigated areas in North American summer rainfall caused by large-scale systems, *J. Appl. Meteorol.*, *37*, 325–331, doi:10.1175/1520-0450-37.3.325.

Sellers, P. J., Y. Mintz, Y. C. Sud, and A. Dalcher (1986), A simple biosphere model (SiB) for use within general circulation models, *J. Atmos. Sci.*, *43*, 505–531, doi:10.1175/1520-0469(1986)043<0505:ASBMFU>2.0.CO;2.

Seneviratne, S. I., et al. (2006), Soil moisture memory in AGCM simulations: Analysis of Global Land-Atmosphere Coupling Experiment (GLACE) data, *J. Hydrometeorol.*, *7*, 1090–1112, doi:10.1175/JHM533.1.

Sun, Y., S. Solomon, A. Dai, and R. W. Portmann (2007), How often will it rain?, *J. Clim.*, *20*, 4801–4818, doi:10.1175/JCLI4263.1.

Tan, P.-H., C. Chou, and J.-Y. Tu (2008), Mechanisms of global warming impacts on robustness of tropical precipitation asymmetry, *J. Clim.*, *21*, 5585–5602, doi:10.1175/2008JCLI2154.1.

Teuling, A. J., S. I. Seneviratne, C. Williams, and P. A. Troch (2006), Observed timescales of evapotranspiration response to soil moisture, *Geophys. Res. Lett.*, *33*, L23403, doi:10.1029/2006GL028178.

van den Hurk, B. J. J. M., et al. (2005), Soil control on runoff response to climate change in regional climate model simulations, *J. Clim.*, *18*, 3536–3551, doi:10.1175/JCLI3471.1.

Wang, G., Y. Kim, and D. Wang (2007), Quantifying the strength of soil moisture-precipitation coupling and its sensitivity to changes in surface water budget, *J. Hydrometeorol.*, *8*, 551–570, doi:10.1175/JHM573.1.

Wu, W., and R. E. Dickinson (2004), Time scales of layered soil moisture memory in the contest of land-atmosphere interaction, *J. Clim.*, *17*, 2752–2764, doi:10.1175/1520-0442(2004)017<2752:TSOLSM>2.0.CO;2.

Xue, Y., and J. Shukla (1993), The influence of land surface properties on Sahel climate. Part I: Desertification, *J. Clim.*, *6*, 2232–2245, doi:10.1175/1520-0442(1993)006<2232:TIOLSP>2.0.CO;2.

Yeh, P. J.-F., and E. A. B. Eltahir (2005a), Representation of water table dynamics in a land surface scheme. Part I: Model development, *J. Clim.*, *18*, 1861–1880, doi:10.1175/JCLI3330.1.

Yeh, P. J.-F., and E. A. B. Eltahir (2005b), Representation of water table dynamics in a land surface scheme. Part II: Subgrid variability, *J. Clim.*, *18*, 1881–1901, doi:10.1175/JCLI3331.1.

Yeh, P. J.-F., and J. S. Famiglietti (2009), Regional groundwater evapotranspiration in Illinois, *J. Hydrometeorol.*, *10*, 464–478, doi:10.1175/2008JHM1018.1.

Yeh, T. C., R. T. Wetherald, and S. Manabe (1984), Effect of soil moisture on the short-term climate and hydrology change: A numerical experiment, *Mon. Weather Rev.*, *112*, 474–490, doi:10.1175/1520-0493(1984)112<0474:TEOSMO>2.0.CO;2.

York, J. P., M. Person, W. J. Gutowski, and T. C. Winter (2002), Putting aquifers into atmospheric simulation models: An example from the Mill Creek Watershed, northeastern Kansas, *Adv. Water Resour.*, *25*, 221–238, doi:10.1016/S0309-1708(01)00021-5.

Yuan, X., Z. Xie, J. Zheng, X. Tian, and Z. Yang (2008), Effects of water table dynamics on regional climate: A case study over east Asian monsoon area, *J. Geophys. Res.*, *113*, D21112, doi:10.1029/2008JD010180.

Zhang, J., W.-C. Wang, and J. Wei (2008), Assessing land-atmosphere coupling using soil moisture from the Global Land Data Assimilation System and observational precipitation, *J. Geophys. Res.*, *113*, D17119, doi:10.1029/2008JD009807.

J. S. Famiglietti and M.-H. Lo, Department of Earth System Science, University of California, Irvine, CA 92697, USA. (jfamigli@uci.edu; mlo@uci.edu)